Multivariate curve resolution applied to *in situ* X-ray absorption spectroscopy data: An efficient tool for data processing and analysis

Alexey Voronov[a], Atsushi Urakawa[b*], Wouter van Beek[c*], Nikolaos E. Tsakoumis[a], Hermann Emerich[c] and Magnus Rønning[a*]

[a] Department of Chemical Engineering, Norwegian University of Science and Technology (NTNU), NO-7491 Trondheim, Norway

[b] Institute of Chemical Research of Catalonia (ICIQ), Tarragona, Spain

[c] The Swiss-Norwegian Beamlines (SNBL) at ESRF, BP 220, F-38043 Grenoble, France

[*] Corresponding authors. E-mail address: aurakawa@iciq.es, wouter@esrf.fr, magnus.ronning@ntnu.no

Abstract

Large datasets containing many spectra commonly associated with *in situ* or *operando* experiments call for new data treatment strategies as conventional scan by scan data analysis methods have become a time-consuming bottleneck. Several convenient automated data processing procedures like least square fitting of reference spectra exist but are based on assumptions. Here we present the application of multivariate curve resolution (MCR) as a blind-source separation method to efficiently process a large data set of an *in situ* X-ray absorption spectroscopy experiment where the sample undergoes a periodic concentration perturbation. MCR was applied to data from a reversible reduction-oxidation reaction of a rhenium promoted cobalt Fischer-Tropsch synthesis catalyst. The MCR algorithm was capable of extracting in a highly automated manner the component spectra with a different kinetic evolution together with their respective concentration profiles without the use of reference spectra. The modulative nature of our experiments allows for averaging of a number of identical

periods and hence an increase in the signal to noise ratio (S/N) which is efficiently exploited by MCR. The practical and added value of the approach in extracting information from large and complex datasets, typical for *in situ* and *operando* studies, is highlighted.

Keywords: X-ray Absorption Spectroscopy, Multivariate Curve Resolution, modulation, in situ, operando.

1. Introduction

During the last two decades many synchrotron beamlines specialized in X-ray absorption spectroscopy (XAS) have increased their instrumental performance enormously. While recording a single spectrum used to take several tens of minutes, now it can be recorded in less than 10 seconds or even in the order of milliseconds [1]. This has opened up the way to perform *in situ* and *operando* XAS experiments with the ambitious aim to shed light on transient structures. In such experiments XAS data are collected as a function of time while changing a variable of the experimental condition such as temperature, concentration, or pressure. It has become routine to collect hundreds of spectra on a single sample. These large datasets have to be treated and the conventional scan by scan data analysis methods have become a time consuming bottleneck. Automated data processing procedures like least square fitting of data with a linear combination (LC) of reference spectra and Principle Component Analysis (PCA) are powerful tools yet have limitations. More precisely LC requires standards and PCA often provides mixed components that are hard to interpret. Here we present the application of multivariate curve resolution (MCR) as a blind-source separation method [2, 3] to process a large data set of an *in situ* XAS experiment where a

sample is under periodic concentration perturbation with simultaneous effluent gas analysis. The advantage of MCR extracted components is that they can be treated as conventional XAS spectra.

In a XAS experiment the X-ray energy is scanned over and beyond the absorption edge and the intensity before and after the sample is recorded. The photo-electrons are ejected from the absorbing atom and interfere with the direct surroundings following many different scattering paths. These paths give rise to an oscillatory, wiggling behavior of the extended X-ray absorption fine structure (EXAFS) signal. By the very nature, the EXAFS spectral response is hence the sum of many overlapping contributions that have to be untangled. When performing *in situ* experiments under chemical and/or structural transformations, the EXAFS signal often consists of contributions from at least two or more species. Due to the aforementioned wiggling nature of EXAFS region in the XAS data, the challenge is to untangle overlapping peaks unequivocally. The difficulty in the separation of heavily overlapping peaks can be mitigated by increasing measurement resolution such as ultrahigh resolution fluorescence analyzer systems [4] which are available only on highly specialized beamlines. Modulation excitation spectroscopy (MES) is a method for transient studies and monitors sensitively and selectively the species or the physical states of interests [5]. MES has been combined with EXAFS to boost the detection sensitivity [1, 6, 7]. By using the mathematical engine of MES, commonly referred to as phase sensitive detection (PSD), great sensitivity enhancement has indeed been demonstrated. However, the wiggling and overlapping nature of EXAFS spectra is not well suited for conventional MES analysis using PSD. The PSD method has difficulty in differentiating heavily overlapping peaks with distinct kinetics. More recently, the spectra after PSD were analyzed by a fitting procedure using reference spectra to

quantitatively understand small spectral changes observed [8]. This is one way of solving the overlap problem of the different components; unfortunately it requires a priori knowledge or assumptions on the changes in the samples and uses reference spectra. Multivariate curve resolution (MCR) analysis on X-ray absorption near edge spectroscopy (XANES) data is slowly getting established and has been applied for battery research [9], for studying substitution reactions in layered hydroxides [10] and the determination of an activation pathway in a copper alumina catalyst [11]. In this paper we present the application of MCR to an *in situ* catalytic EXAFS study with a periodic gas concentration modulation. In the present work MCR - alternating least squares (ALS) was used for the blind separation of the spectral components. With blind we mean without any standards or any other input information except the data (i.e. spectra) matrix itself. The blind source is a great advantage of the MCR because only experimental data are needed and no prior assumptions have to be made for the analysis.

2. Material and methods

2.1. MCR applied to XAS data

In this work the MCR methodology has been directly applied to the time-resolved XAS data: **D** is the data matrix of $m \times n$ in size, where m is the number of recorded spectra and n is the number of the data points in energy scale in XAS. The information about the spectra of individual components and their concentrations or populations can be extracted by solving the component resolution problem [12]. In order to do so the matrix of raw spectra **D** has to be decomposed into bilinear contributions of the pure components, i.e. concentration profiles, and spectra [13]. Equation (1) shows that in MCR data matrix **D** is expressed by three matrices **C**, **S**, and **E**. **C**($m \times k$) is the matrix

where its columns contain the concentration variations or kinetic profiles of k pure components during the transformation. $\mathbf{S}(n \times k)$ contains the columns of the respective spectra of the pure components. The main goal of MCR is to determine the **C** and **S** matrices only by analyzing the data matrix [14]. It is also important to note that the term 'pure components' denotes a group of features that varies with a unique pattern, compared to other responses coming from the sample. It does not necessarily have to be a chemically pure component but could e.g. represent a mixture of chemically pure components as long as they behave together (kinetically) in the same manner. The third term $\mathbf{E}(m \times n)$ is a matrix with leftover unexplained signal after the multiplication of the concentration **C** and component $\mathbf{S}^T$ matrices. Ideally the **E** matrix would contain the experimental uncertainties.

$$\mathbf{D} = \mathbf{C}\mathbf{S}^T + \mathbf{E} \quad (1)$$

Equation 1 is solved iteratively by finding the optimal combination of the **C** and **S** matrices using least squares optimization on the **E** variance matrix. This technique has been successfully applied in a great deal of analytical problems[15-18]. Typical MCR-ALS steps have been reported elsewhere[13]. In order to increase the MCR performance, physically logical constraints can be employed in the decomposition procedure[14, 19]. For instance positive values for concentrations as well as spectral profiles are used as constraints for common spectral analyses. This is one of the advantages of MCR over PCA because the latter uses statistical criteria during component extraction resulting in components more difficult to interpret.

It should be underlined that we employed the MCR-ALS on XAS data as a blind source separation tool to extract pure component spectra and their respective concentration profiles. However, other blind source separation algorithms do exist with imposed component independence criteria, and the origin of the criteria differs in

MCR-ALS. MCR-ALS should hence not be taken as a general or sole solution for blind source separation, although it did perform well in this application compared to independent component analysis (ICA), such as SNICA [2], in this particular case.

The MCR algorithm has been developed, described and discussed in detail by Tauler et al. [19-23]. Multivariate resolution methods also assume that the experimental data follows Lambert-Beer's law. This assumed linearity between recorded spectral data and component concentrations is widely accepted for XAS data [24, 25]. Hence our aim is to extract the concentration **C** and spectra **S** matrices from only the experimental data matrix **D** without using any reference spectra. Before extracting the **C** and **S** matrices the number of pure components present in the system needs to be defined. Then initial estimations of matrices **C** and **S** have to be obtained from the techniques based on the evolving factor analysis [14, 19, 20, 22, 23, 26, 27]. Later, the iteration mechanism comes into play. A new estimation of the matrices **C** and **S** is obtained after each iteration (equations 2 and 3).

$$\mathbf{C}^{+}\mathbf{D}^{*}=\mathbf{C}^{+}\mathbf{C}\mathbf{S}^{T}=\mathbf{S}^{T} \quad (2)$$

$$\mathbf{D}^{*}(\mathbf{S}^{T})^{+}=\mathbf{C}(\mathbf{S}^{T})(\mathbf{S}^{T})^{+}=\mathbf{C} \quad (3)$$

Matrix **D*** is the data matrix produced by principal component analysis (PCA) [27] for the selected number of components. Matrix $\mathbf{C}^{+}$ is the pseudo-inverse (as matrix C is not necessarily square) of matrix **C** and $(\mathbf{S}^{T})^{+}$ is the pseudo-inverse of the matrix $\mathbf{S}^{T}$. Iterative optimization is performed until convergence is achieved or a specified number of iterations is reached.

2.2. Sample preparation

A Fischer-Tropsch synthesis catalyst, cobalt-rhenium supported on high surface area γ-Al_2O_3, was chosen as our model system [28]. The catalysts were prepared by a co-impregnation technique. Cobalt nitrate hexahydrate and perrhenic acid were dissolved

in de-ionized water and the solution was impregnated on γ-Al_2O_3. The catalysts were dried in air for 3 hours at 393 K followed by calcination in air for 16 hours at 573 K. The average cobalt particle size was ca. 8-10 nm with 20 wt% of cobalt. Sieved catalyst fractions of 53-90 μm were used for the experiments.

2.3. XAS measurements

XAS experiments were performed on BM01B at the Swiss-Norwegian Beamlines (SNBL) of the European Synchrotron Radiation Facility (ESRF), France. XAS spectra were recorded at the cobalt K-edge (7709 eV) with a double crystal Si(111) monochromator. A cobalt foil was used for energy calibration. The first inflection point was calibrated to the Co K-edge energy. All measurements were performed in transmission mode. Gas filled ion chambers before and after the sample were used to measure the XAS signal.

XAS spectra were recorded near the Co K-edge (7709 eV) with 1 eV energy step in continuous scanning mode. One spectrum was recorded in about 31 seconds. 6 oxidation-reduction cycles were taken in total. Each cycle consists of 30 spectra (15 spectra under H_2 flow and subsequent 15 spectra in the flow of the O_2 in He).

2.4. Reaction and setup description

A reversible oxidation-reduction reaction of the Co component of the Fischer-Tropsch synthesis catalyst was used to test the MCR methodology. The experimental setup is shown in Fig. 1.

Gas flows were controlled by mass flow controllers. One of the key elements of the setup is the switching valve. The switching valve allowed rapid switching (< 200 ms) between two gas lines containing either 2.5 mL/min of H_2 (99.999 %) or O_2 in He (2.2mL/min He + 0.3 mL/min O_2). The pressure in both lines (sample and blank) was adjusted to ambient pressure by back pressure controllers. Equalizing the pressure in

both lines is very important as it enables a sharp and clean switching front between the gases. A quartz capillary (OD: 1 mm, wall thickness 20 μm) [28] was used as the *in situ* reactor cell. The temperature was set to 488 K. The concentrations of gaseous components after the reactor cell were monitored by a mass spectrometer (Pfeiffer Vacuum, OmniStar) in order to verify whether the envisaged reaction actually took place throughout the whole experiment.

2.5. Data analysis

2.5.1. Pre-treatment

In a time resolved experiment one always needs to make a trade-off between time resolution and S/N. Increasing time resolution leads to a decrease in S/N and vice versa. As the oxidation-reduction reaction induced by switching between oxygen and hydrogen atmospheres is a reversible process, one can repeatedly scan the changes upon gas switching while recording the spectra with a required time resolution to capture the spectral evolution of interest in spite of possibly insufficient S/N of each scan for proper spectral analysis. The obtained multi-cycle data can be averaged into one cycle to improve S/N and the degree of the improvement, according to Gaussian statistics, is proportional to the number of cycles which is an experimental parameter. This post-averaging scheme can be very practical in reducing the data size for further analysis like MCR-ALS in the light of availability of modern detectors with high spectral resolution and fast scan capability. A detailed analysis of the S/N improvement is given in the Supplementary Material.

Prior to the averaging procedure the studied system should be allowed to reach a quasi steady-state [5]. In Fig. 2a, the first three cycles of the experimental data during O_2-H_2 switching are shown. It becomes immediately clear that the spectral response in the first cycle is different from that of the second and third cycles. Before the initial cycle

198 which starts from the oxygen atmosphere, the sample was freshly reduced. The state of
199 the catalyst and/or the degree of Co reduction is different after exposing to O_2 flow.
200 From the second cycle onwards the temporal response of the spectra at each cycle was
201 identical (Fig. 2b), thus a quasi steady-state was reached after the first cycle. This is
202 also confirmed by the MS response (see Supplementary Material). Hence the spectra
203 of the 5 cycles, from the 2nd until the 6th cycle, were averaged into one cycle. All data
204 pre-treatment procedures were performed using MATLAB software. As a result, one
205 averaged cycle is produced with significantly improved S/N (Fig. 2c). The averaged
206 EXAFS data were used for data processing by MCR.

207 **2.5.2. Conventional versus MCR data processing**

208 Conventional EXAFS data processing includes several initial steps such as
209 normalization, background subtraction and edge position correction. Fig. 3 shows the
210 Fourier transforms of the averaged EXAFS spectra (i.e. one cycle) after the pre-
211 processing steps (details given in Supplementary Material).

212 All the transformed spectra are apparently different from each other, meaning that all
213 30 spectra must be processed and analyzed separately. This is a time-consuming
214 procedure and becomes impractical for large datasets. Note that this is still a relatively
215 small dataset compared to the experimental capabilities of state of the art XAS stations.
216 MCR works differently; here the entire system is represented by the various
217 components present in the system and their concentrations. Fig. 4 graphically
218 represents the result of the MCR method applied to our XAS data. The commercially
219 available Unscrambler X 10.2 software was used for the MCR data analysis. We have
220 constrained the MCR analysis to non-negativity for spectra and concentration profiles.
221 Here the data matrix **D** is expressed by the matrices of "MCR pure component"
222 spectra **S** and their concentrations **C** varying with time and the associated residual

error **E** matrix (shown in Supplementary Material). In this particular example only two components and their concentration profiles were, at the first glance, sufficient to represent the data with very little residual error. Therefore compared to conventional EXAFS data treatment, only 2 spectra need to be interpreted instead of 30. In conventional EXAFS data analysis each of the 30 datasets would be compared or fitted with parameters from a proposed structural model. Alternatively, the spectra can be fitted by a linear combination of chemically pure standard spectra (typical for XANES analysis). By doing so a model is forced into the interpretation such that variations have to occur by going directly from one to another chemically pure component. With the MCR-ALS methodology the varying components are extracted based on kinetic correlations in the data *without* any assumptions on chemical pureness. If a system would respond from one chemically pure bulk component to another, both traditional and MCR methods would give the same result. MCR analysis would still come with the speed of data-analysis advantage. However, if bulk references do not describe the transient structures in the data properly MCR would be able to show this effectively where reference based methods would fail. In other terms, MCR-ALS would be able to identify species and components in samples for which references are not available.

Quantification with MCR is possible but care has to be taken because the multiplication of a component spectrum and its concentration yields the actual intensity of the decomposed spectra. Therefore the concentrations obtained by MCR should be scaled by the intensity of the component spectrum of a reference with known concentration.

Furthermore, it has to be mentioned that the averaged dataset, absorption coefficient (mu) as a function of X-ray energy and time, is processed by the MCR-ALS algorithm.

The physically more meaningful interpretation is done only after standard EXAFS analysis, in brief Fourier transform, on the MCR-ALS extracted component spectra.

2.5.3 Number of pure components

The MCR implementation in Unscrambler performs PCA before MCR processing to define the number of components. For this particular example Unscrambler yielded two data sets: one with 2 and the other with 3 pure components, with a suggestion for the former based on a statistical criterion (see Supplementary Material). The question is: Can the 2 components be regarded as the solution? Indeed, the explained variance with 2 components is already above 99.9 % and the two component model can reasonably explain the spectral shape and evolution as one can see in the results and discussion section. However, it should be noted that a variety of statistical stopping rules for defining the number of components exist [29]. Looking in great detail at the individual PCA loadings (Supplementary Material), one can clearly observe the high S/N spectral structure in the 1st, 2nd, and also 3rd component, whereas the 4th and above components are dominated by noise. The statistical analysis in the Supplementary Material reports the quality of fit in terms of total residues for the 2- and 3-component analysis. It is worth mentioning that the identical conclusions can be drawn without averaging the data and processing either the last 5 cycles or all 6 cycles (Supplementary Material). The number of components selected for the determination of the pure component spectra is of primary importance for the final interpretation of the data and here we find it valuable and useful to examine the S/N and spectral structure using PCA to determine the number of pure components to be included in the MCR analysis. From the statistical analysis and the data interpretation it is evident that all low-noise components need to be examined for meaningful chemical interpretation.

In this work, we present both cases as an illustration of both 2- and 3-component cases and potential pitfalls in using MCR for blind source spectral separation.

3. Results and discussion

The MCR procedure delivers individual component spectra that can be processed as conventional EXAFS spectra. To illustrate this, we first perform the EXAFS analysis on a simple example, namely the 2 component MCR decomposition, suggested as the likely solution based on the statistical criteria. By showing the incomplete 2 component example (Section 2.5.3) we also intend to sensitize potential users of the method about the extreme importance of careful number component selection.

In Fig. 4 typical profiles of X-ray absorption spectra after MCR decomposition are shown. The part of the components spectra which can be processed for detailed EXAFS analysis (ca. 50 eV above the edge) has the typical oscillating nature. Fig. 5 shows raw and normalized Fourier transformed spectra of the 2 components without phase-correction obtained after the MCR treatment.

Component 1 has a magnitude approximately 15 times higher than component 2. The large difference between FT magnitudes of the two components is due to the difference in the intensities of the oscillating parts of the components spectra **S** (Fig. 4). It should be reminded that the actual signal intensity of the component spectra can be retrieved by its multiplication with the corresponding concentration. This means that the actual difference in their intensities is not as large as shown in Fig. 5a because component 2 has lower intensity with higher concentration throughout the O_2-H_2 cycle. It is interesting to note that the concentration of component 2 changes but remains high, while that of component 1 diminishes completely at around the 10th spectrum (C in Fig. 4). For the sake of clear comparison between the two components,

FT curves were normalized to the highest peak. Fig. 5b shows that there is a significant difference between the components, implying that the two components belong to the substances with different chemical and structural nature. For a better understanding of the chemical meaning of the components, the FT curves of the two components and of the cobalt containing standards are compared (Fig. 6).

The most intense peak of component 1 clearly resembles the main peak of cobalt metal. Hence we can conclude that component 1 has mainly metallic nature. On the other hand, the assignment of component 2 is more ambiguous and it apparently consists of a mixture of Co_3O_4 and CoO. No peak of metallic cobalt was detected comparing the spectra of the component 2 and of metallic cobalt. Therefore MCR can clearly separate the metallic component of the studied sample from the component containing oxidized cobalt. This suggests that the components represent features with a clear chemical meaning. In Fig. 4 the concentration matrix **C** is presented as a concentration plot. As mentioned earlier, the concentration of component 1 drops close to zero after the 10th scan in O_2 flow but it increases again after a while when switching to H_2 flow. The concentration profile of component 2 behaves in an opposite manner to that of component 1 albeit at a higher concentration level as mentioned earlier. The concentration profiles are also chemically reasonable because components 1 and 2 correspond to metallic Co and Co oxides, respectively, according to Fig. 6. By visual inspection of the XAS edge profiles in Fig. 3 the close to zero concentration of metallic Co and the rather high concentration variations indicates that the majority of the cobalt in the catalyst alternates between metallic cobalt (in H_2) and cobalt oxides (in O_2) throughout the cycle.

As explained in Section 2.5.3 and in the Supplementary Material, the presence of 3 components can be concluded based on the structure of scores and S/N of loadings in

PCA. Also when we increase the number of components to three, the sum of all differences in matrix **E** is reduced by a factor of 40 (Supplementary Material), but does the increase in the number of components make better chemical sense and does MCR hence provide more detailed information?

The next example uses the same XAS data set but separated into 3 components by MCR. In Fig. 7 the component spectra and the corresponding concentration profiles after decomposition into 3 components are presented.

The component concentration profiles look similar to those obtained after decomposition into 2 components (Fig. 4) except for the presence of the additional profile of component 2.

Note that the number of components used in the extraction is an important parameter to be precisely determined, as it could also have a large effect on the shape of extracted components. Again, for better understanding of chemical transitions, analysis of the Fourier transforms of the extracted components was performed first. Conventional data processing including the background subtraction, edge shift and normalization was done prior to Fourier transformation. A comparison is shown in Fig. 8. Component 1 mainly represents the metallic part of the system (a) while components 2 and 3 show the presence of cobalt oxides. Component 3 resembles pure Co_3O_4 (b) whereas component 2 represents the structure of an intermediate between CoO and Co_3O_4 when comparing the positions and intensities. According to the component concentration profiles, the oxidation-reduction process for the cobalt can be explained in the following way: After introduction of oxygen, the surface cobalt atoms are oxidized with the initial formation of CoO. Co_3O_4 is formed at the expense of CoO (Fig. 7b, 8-10th scan number). After switching to hydrogen flow Co_3O_4 is partially reduced to CoO (Fig. 7b, 17-20th scan number). The concentration of the

metallic component is increased gradually after the introduction of hydrogen together with a simultaneous decrease in the concentrations of both CoO and Co_3O_4.

The MCR analysis shows that oxidation of cobalt is a two-step process with the Co_3O_4 as the resulting oxide and CoO as an intermediate component. This shows that the oxidation of cobalt follows the same mechanism as observed for the reduction of Co_3O_4 crystallites in traditional XANES analysis in previous studies [30]. An additional validation of the blind source separation method was performed by comparing results of EXAFS and XANES MCR analysis with and without an initial guess on the pure components using references spectra of bulk Co, CoO and Co_3O_4. The results of these extractions are given in the Supplementary Material. It can be seen that all concentration profiles show the same trends, confirming the validity of MCR as the blind source separation method.

Does the information extracted by MCR-ALS go beyond the traditional methods? It is clear from Fig. 8 that the extracted components do not fully match with the EXAFS reference spectra. This shows that the MCR-extracted components do not necessarily represent bulk chemical phases, which could be explained as follows: The changes in the cobalt particles during oxidation-reduction cycles are of transient character and the system is highly dynamic. The mixed character of CoO and Co_3O_4 observed for component 2 may be caused by the transient nature of the oxide phases and that nanoparticles were used in this study (ca. 8-10 nm in size). The surface fraction of Co atoms gives a significant contribution to the overall signal. Hence it becomes clear that the cobalt species in our study are not well described by the bulk reference compounds. This also demonstrates the obvious limitations of traditional LC analysis of XANES spectra using such reference compounds. Better time resolution, providing finer sampling, might increase the accuracy of the MCR analysis. Further work is

needed to study the influences of sampling rates on the quality of MCR-ALS extractions and to provide clear experimental guidelines to optimize such experiments. It is also worth noting that, thanks to the modulative nature of our experiments, the detection limits as well as the data size can be pushed down by averaging many cycles. The latter data size reduction advantage can be very practical considering the increasing availability of modern high resolution, fast detectors. Especially in catalysis research, where the active species often represents only a minute (surface) fraction of the overall catalytic body, the presented modulation -> averaging -> MCR-ALS approach might be able to provide new experimental insights. The represented data already shows the power of the methodology in efficient and insightful EXAFS data analysis for catalysis research.

4. Conclusions

The application of MCR to X-ray absorption spectroscopy data has been demonstrated on a modulated oxidation-reduction treatment of cobalt-based Fischer-Tropsch synthesis catalysts. The complex hardware needed for such experiments has been described in detail. **MCR was capable of extracting in a highly automated manner component spectra with distinct kinetic evolution together with their respective concentration profiles without the use of reference spectra.** Great care has to be taken in the selection of the number of pure components. Comparisons between blind source component extractions and extractions including an initial guess of the components show very similar results providing confidence in the method. The blind extracted components can also be treated with standard software for EXAFS spectral analysis. When comparing the MCR extracted components with bulk references they are somewhat different. This is likely due to the dynamic nature of the system and the nanoparticles used illustrating that bulk references are not representative for the

changes occurring in highly dispersed systems. Furthermore it is demonstrated that the components extracted with MCR have a clear chemical meaning and, together with their concentration profile, explain the transformation mechanism of the redox reaction in detail. Hence MCR is capable of automatically extracting unbiased chemically meaningful component spectra together with their concentration profiles from large *in situ* XAS datasets.

Acknowledgements

This publication forms a part of the inGAP (Innovative Natural Gas Processes and Products) Centre of Research-based Innovation, which receives financial support from the Research Council of Norway under contract no. 174893. The authors would like to thank the Research Council of Norway for financial support through the KOSK-II and SYNKNØYT programmes and Statoil for financial support through the inGAP project. The project team of the Swiss-Norwegian Beamlines is highly acknowledged for experimental assistance. We thank anonymous reviewers for valuable suggestions helping us to improve the manuscript substantially.

References

1. D. Ferri, M. S. Kumar, R. Wirz, A. Eyssler, O. Korsak, P. Hug, A. Weidenkaff and M. A. Newton, *Physical Chemistry Chemical Physics*, 2010, **12**, 5634-5646.
2. Y. B. Monakhova, S. A. Astakhov, A. Kraskov and S. P. Mushtakova, *Chemometrics and Intelligent Laboratory Systems*, 2010, **103**, 108-115.
3. Y. B. Monakhova, S. A. Astakhov, S. P. Mushtakova and L. A. Gribov, *Journal of Analytical Chemistry*, 2011, **66**, 351-362.
4. F. de Groot, *Chemical Reviews*, 2001, **101**, 1779-1808.
5. A. Urakawa, T. Bürgi and A. Baiker, *Chemical Engineering Science*, 2008, **63**, 4902-4909.
6. D. Ferri, M. Newton and M. Nachtegaal, *Topics in Catalysis*, 2011, **54**, 1070-1078.
7. A. Eyssler, E. Kleymenov, A. Kupferschmid, M. Nachtegaal, M. S. Kumar, P. Hug, A. Weidenkaff and D. Ferri, *The Journal of Physical Chemistry C*, 2010, **115**, 1231-1239.
8. C. F. J. König, J. A. van Bokhoven, T. J. Schildhauer and M. Nachtegaal, *The Journal of Physical Chemistry C*, 2012, **116**, 19857-19866.
9. P. Conti, S. Zamponi, M. Giorgetti, M. Berrettoni and W. H. Smyrl, *Analytical Chemistry*, 2010, **82**, 3629-3635.
10. H. W. P. Carvalho, S. H. Pulcinelli, C. V. Santilli, F. Leroux, F. Meneau and V. Briois, *Chemistry of Materials*, 2013, **25**, 2855-2867.

11. W. H. Cassinelli, L. Martins, A. R. Passos, S. H. Pulcinelli, C. V. Santilli, A. Rochet and V. Briois, *Catalysis Today*, 2014, **229**, 114-122.
12. I. H. M. van Stokkum, K. M. Mullen and V. V. Mihaleva, *Chemometrics and Intelligent Laboratory Systems*, 2009, **95**, 150-163.
13. L. Blanchet, A. Mezzetti, C. Ruckebusch, J. P. Huvenne and A. De Juan, *Analytical and Bioanalytical Chemistry*, 2007, **387**, 1863-1873.
14. W. Kessler, D. Oelkrug and R. Kessler, *Analytica Chimica Acta*, 2009, **642**, 127-134.
15. T. Azzouz and R. Tauler, *Talanta*, 2008, **74**, 1201-1210.
16. M. J. Culzoni, A. Mancha de Llanos, M. M. De Zan, A. Espinosa-Mansilla, F. Cañada-Cañada, A. Muñoz de la Peña and H. C. Goicoechea, *Talanta*, 2011, **85**, 2368-2374.
17. M. Garrido, F. X. Rius and M. S. Larrechi, *Analytical and Bioanalytical Chemistry*, 2008, **390**, 2059-2066.
18. Y. Le Dréau, N. Dupuy, J. Artaud, D. Ollivier and J. Kister, *Talanta*, 2009, **77**, 1748-1756.
19. A. De Juan and R. Tauler, *Analytica Chimica Acta*, 2003, **500**, 195-210.
20. A. de Juan, Y. Vander Heyden, R. Tauler and D. L. Massart, *Analytica Chimica Acta*, 1997, **346**, 307-318.
21. R. Tauler, *Chemometrics and Intelligent Laboratory Systems*, 1995, **30**, 133-146.
22. R. Tauler and D. Barceló, *TrAC Trends in Analytical Chemistry*, 1993, **12**, 319-327.
23. R. Tauler, S. Lacorte and D. Barceló, *Journal of Chromatography A*, 1996, **730**, 177-183.
24. S. Ahn, S. Y. Jung, J. P. Lee and S. J. Lee, *Contrast Media & Molecular Imaging*, 2011, **6**, 437-448.
25. J. Als-Nielsen and D. McMorrow, in *Elements of Modern X-ray Physics*, John Wiley & Sons, Inc., 2011, pp. 239-273.
26. M. Maeder and A. Zilian, *Chemometrics and Intelligent Laboratory Systems*, 1988, **3**, 205-213.
27. S. Wold, K. Esbensen and P. Geladi, *Chemometrics and Intelligent Laboratory Systems*, 1987, **2**, 37-52.
28. N. E. Tsakoumis, A. Voronov, M. Rønning, W. v. Beek, Ø. Borg, E. Rytter and A. Holmen, *Journal of Catalysis*, 2012, **291**, 138-148.
29. P. R. Peres-Neto, D. A. Jackson and K. M. Somers, *Computational Statistics & Data Analysis*, 2005, **49**, 974-997.
30. M. Rønning, N. E. Tsakoumis, A. Voronov, R. E. Johnsen, P. Norby, W. van Beek, Ø. Borg, E. Rytter and A. Holmen, *Catalysis Today*, 2010, **155**, 289-295.

Figures

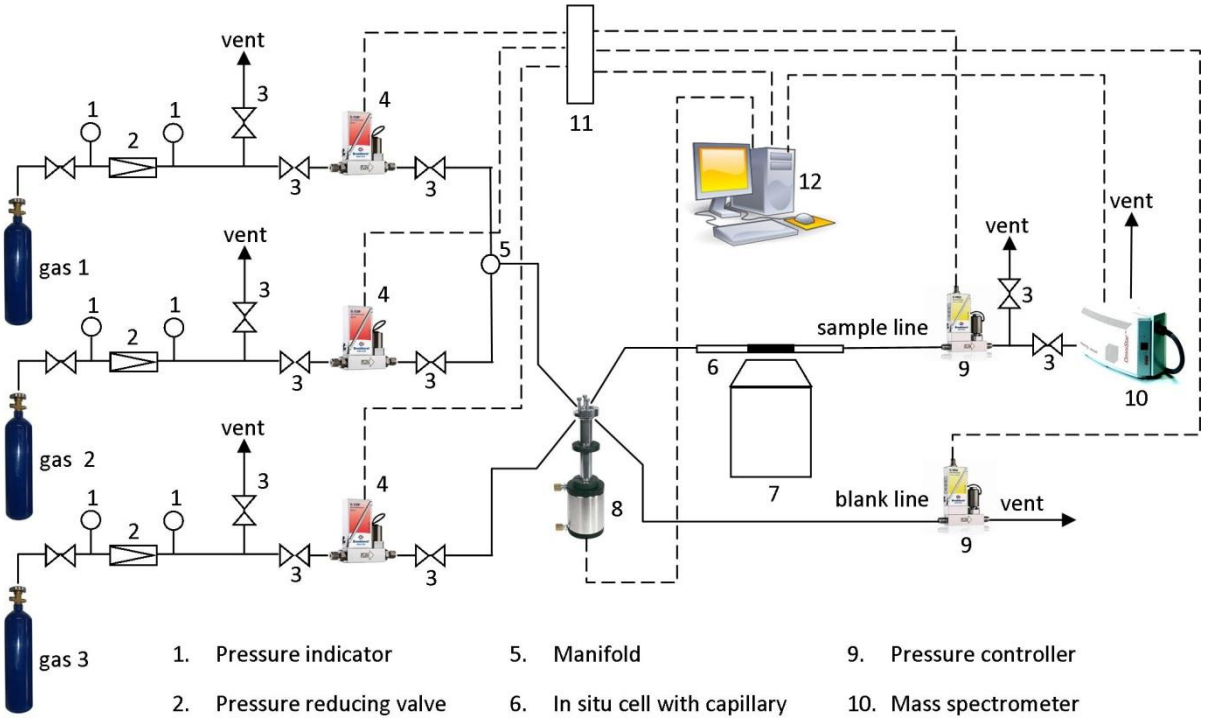

Figure 1. Scheme of the experimental setup used in the experiments.

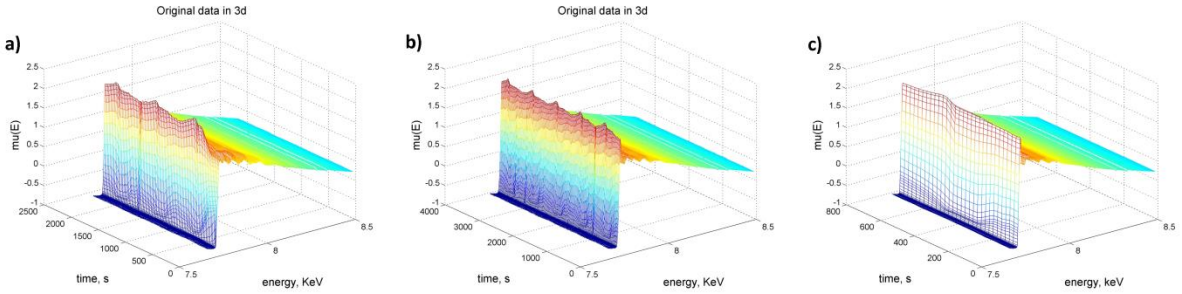

Figure 2. Data pre-treatment steps: a) detection of the quasi steady-state; b) chosen cycles for averaging; c) averaged cycle. The first half of the cycle is under O_2-flow whereas the second half is under H_2-flow.

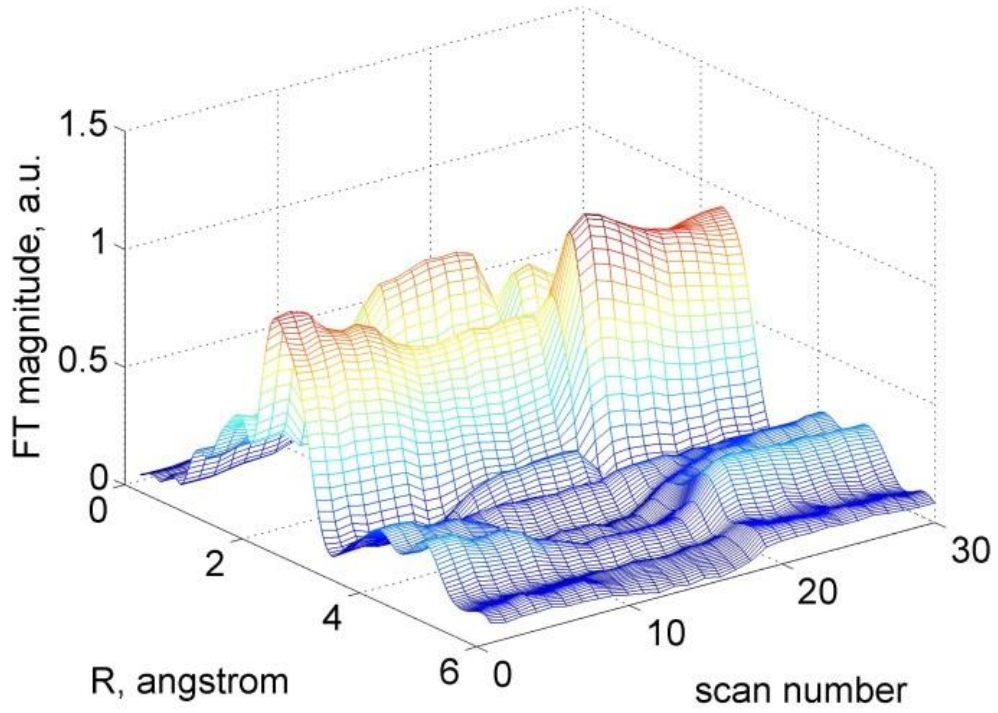

474

475 Figure 3. Fourier transforms of the averaged EXAFS spectra.

476

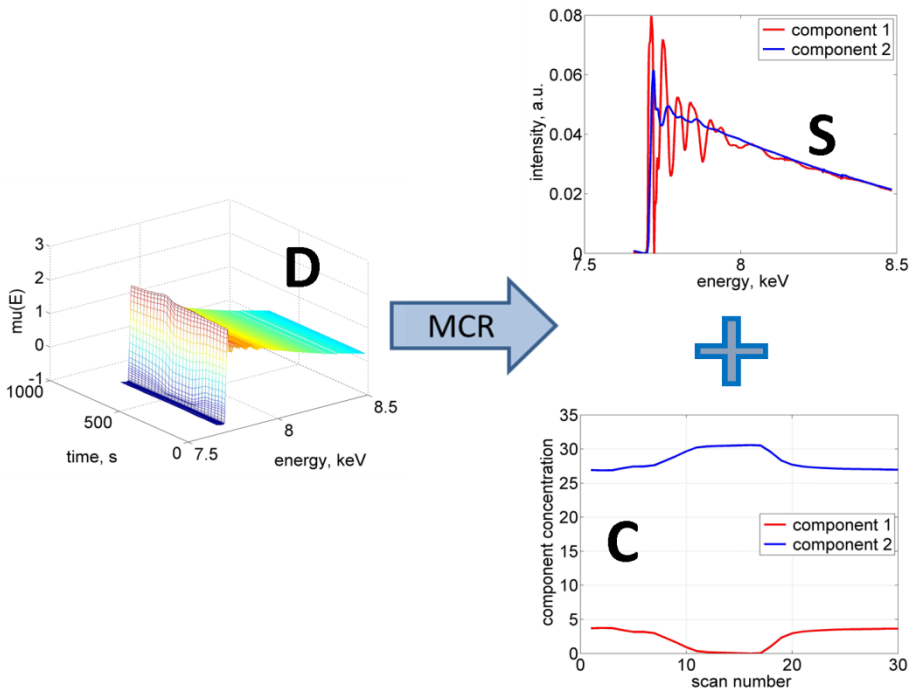

477

478 Figure 4. Graphical representation of eq. (1) using the collected and averaged XAS

479 data.

480

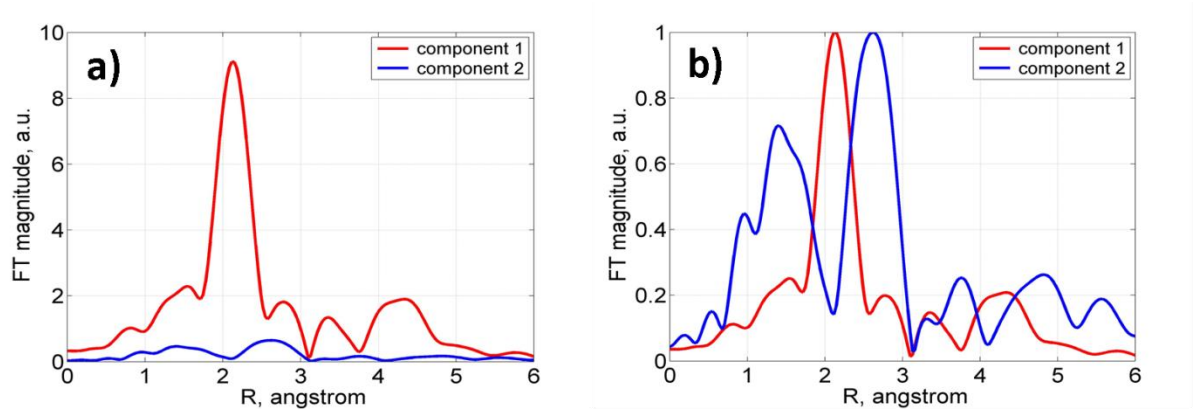

481

482 Figure 5. a) Raw and b) normalized Fourier transformed component spectra obtained

483 after MCR.

484

485 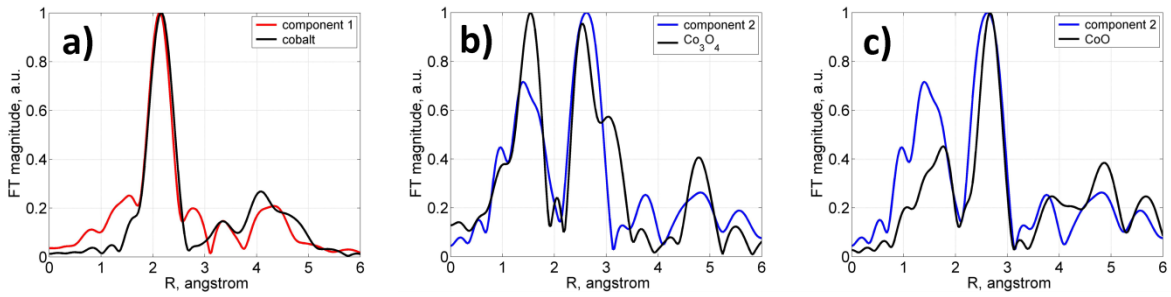

486 Figure 6. Comparison between components and standards: a) component 1 and

487 metallic cobalt; b) component 2 and Co_3O_4; c) component 2 and CoO.

488

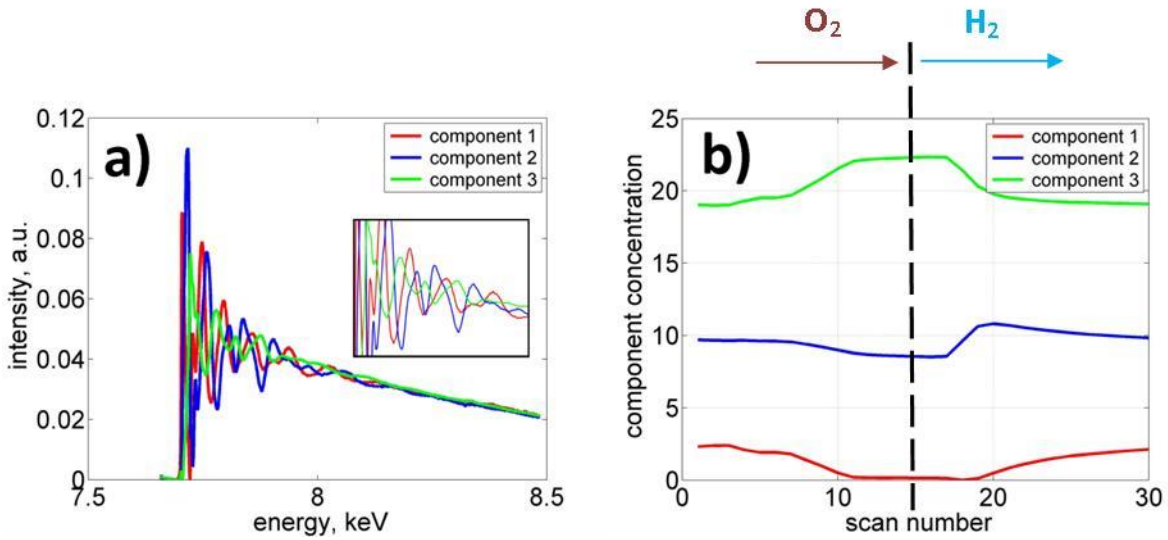

Figure 7. XAS spectra (a) and concentration profiles (b) obtained by MCR where the averaged data (Fig. 2c) was decomposed into 3 components.

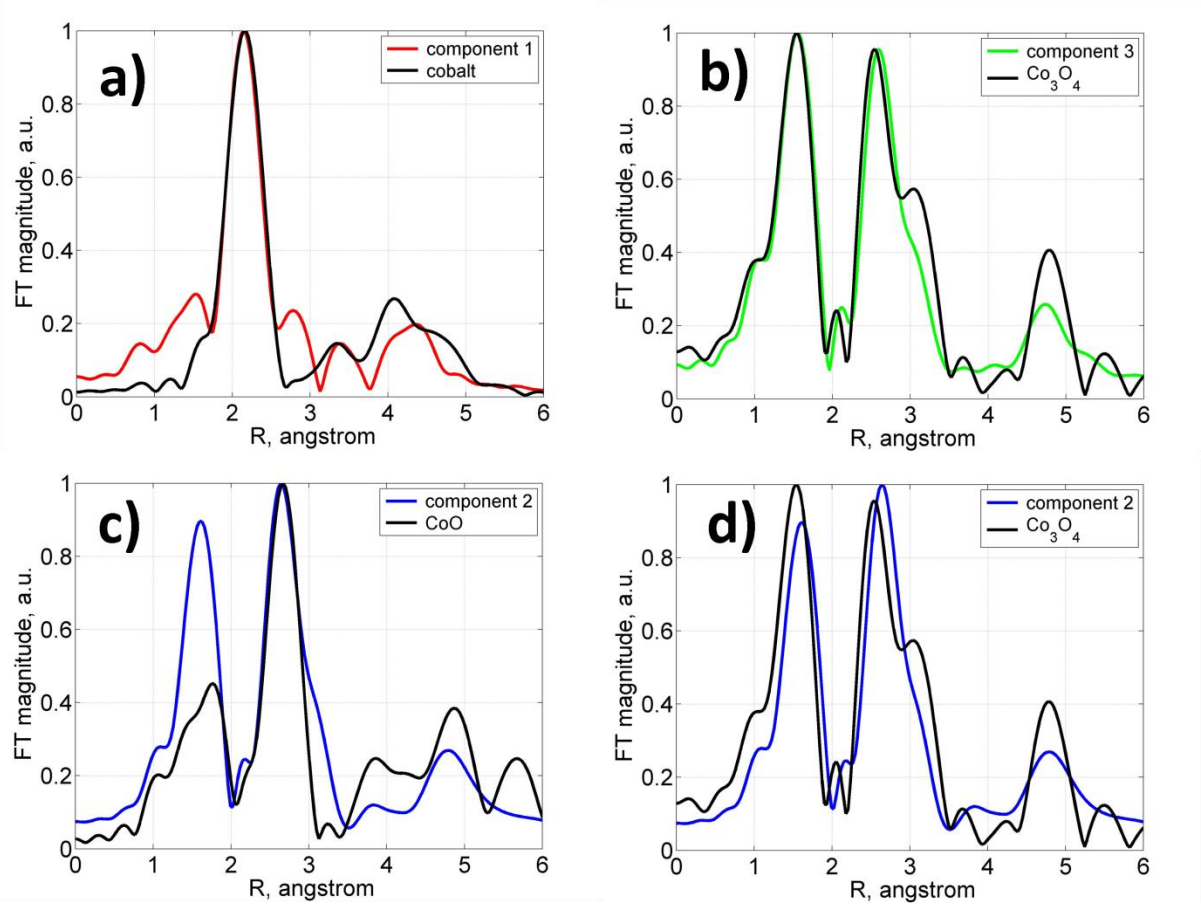

493

494 Figure 8. Comparison between components and standards: a) component 1 and

495 metallic cobalt; b) component 3 and Co_3O_4; c) component 2 and CoO; d) component 2

496 and Co_3O_4.

497

498